Mesophase Identifications in a Series of Liquid Crystalline TPP Polyethers and Copolyethers Having Highly Ordered Mesophase Structures. 2. Phase Diagram of Even-Numbered Polyethers

Yeocheol Yoon, Rong-Ming Ho, Bongseok Moon, Doyun Kim, Kevin W. McCreight, Fuming Li, Frank W. Harris, and Stephen Z. D. Cheng*

Maurice Morton Institute and Department of Polymer Science, The University of Akron, Akron, Ohio 44325-3909

Virgil Percec and Peihwei Chu

Department of Macromolecular Science, Case Western Reserve University, Cleveland, Ohio 44106-2699

Received November 27, 1995; Revised Manuscript Received February 12, 1996[⊗]

ABSTRACT: Liquid crystalline polyethers have been synthesized from 1-(4-hydroxy-4′-biphenylyl)-2-(4-hydroxyphenyl)propane and α,ω-dibromoalkanes with even-numbers of methylene units [TPP(n = even)s]. Multiple phase transitions are found during cooling and heating *via* differential scanning calorimetry (DSC), and they show little undercooling dependence. Ordered structure identifications are based on experimental observations of wide angle X-ray powder and fiber diffraction experiments at different temperatures. Polarized light and transmission electron microscopy observations on mesophase morphology combined with DSC results on thermodynamic transition properties also provide additional evidence for these phase assignments. Moreover, the contributions of the mesogenic groups and the methylene units to each ordering process are obtained based on the changes of transition enthalpy and entropy. In TPP($n \leq 8$)s the highest temperature transition is from the isotropic melt to a nematic phase. This nematic phase is only stable in a narrow temperature range. For instance, it is 12 °C for TPP($n = 4$) and 6 °C for TPP($n = 8$). When the number of methylene units $n \geq 10$, the isotropic melt directly enters a smectic F phase. The second transition in TPP($n \leq 8$)s is from the nematic to the smectic F phase. As a result, the smectic F phase exists for all TPP(n = even)s. Decreasing the temperature further leads to another transition in TPP(n = even)s to form a smectic crystal G phase which is followed by a transition to a smectic crystal H phase. This smectic crystal H phase remains for TPP($n \leq 8$)s down to their glass transition temperatures, while in TPP($n \geq 10$)s further ordering processes occur and crystal phases are observed. A phase diagram of TPP(n = even)s is constructed.

Introduction

In previous publications, we have reported a series of main-chain liquid crystalline polyethers, synthesized from 1-(4-hydroxy-4′-biphenylyl)-2-(4-hydroxyphenyl)-propane and α,ω-dibromoalkanes with odd-numbered methylene units [TPP(n = odd)s], that shows complicated transition behavior.[1−3] Based on our careful structural and thermodynamic transition property analyses as well as the morphological observations, highly ordered smectic structures [smectic F (S_F), smectic crystal G (S_G), and smectic crystal H (S_H) phases] have been recognized. This is one of the first reports in which a liquid crystalline order higher than the smectic A or C phase has been identified in main-chain liquid crystalline polymers.[1−6] As pointed out recently, the highly ordered S_G and S_H phases in small molecule liquid crystals are not truly smectics but rather crystals.[7] We still keep the nomenclature in order to distinguish these phases from polymer lamellar crystals.

The structural recognition of these phases is mainly based on the experimental observation that a layer structure in the low-angle region and sharp reflections in the high-angle region appear from the wide angle X-ray diffraction (WAXD) powder patterns. This is further identified by the WAXD fiber patterns which provide the dimensionality of the order. For TPP(n = odd)s, it has been found that phenomenologically in the highly ordered smectic phases their lateral structure shows "long range order"[8] (correlation length > 10 nm) or "quasi-long range order"[8] (correlation length between 2 and 10 nm) within the layers[1,2] in addition to the layer structure. This suggests that although the long-chain molecules possess covalent connectivity between mesogenic groups and methylene units, it may still be sufficient to classify the phase behavior using the concepts established in small molecule liquid crystals.[9,10]

In this publication, we attempt to complete the structural identification of this series of polyethers by focusing on the phase structures and transitions of the TPPs with even-numbered methylene units [TPP(n = even)s]. These results are based on our differential scanning calorimetry (DSC) experiments to investigate the phase transition thermodynamics, WAXD experiments to identify the ordered structures and follow the structural changes during the transitions, and polarized light and transmission electron microscopy (PLM and TEM) to observe liquid crystalline morphology. It will be shown that in these TPP(n = even) polyethers, highly ordered smectic phases can also be identified, which possess laterally ordered structures higher than smectic

* To whom correspondence should be addressed.
[⊗] Abstract published in *Advance ACS Abstracts,* April 1, 1996.

S0024-9297(95)01746-3 CCC: $12.00

Table 1. Molecular Parameters for TPPs in THF[a]

n	M_n	M_w/M_n	*n*	M_n	M_w/M_n
4[b]			14	16 500	2.03
6[b]			16	28 700	3.42
8[b]			18	23 500	2.92
10	19 700	3.32	20	37 300	2.28
12	18 300	2.90			

[a] The number- and weight-average molecular weights were determined using polystyrene standards. [b] The samples were insoluble.

A or C (S_A or S_C). In other words, their lateral packing order is greater than the short range, liquid-like order. The chemical structures of TPP(n = even)s are

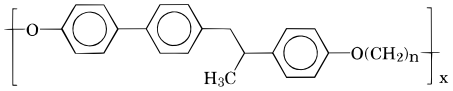

Experimental Section

Materials. TPP(n = even)s were synthesized from 1-(4-hydroxy-4′-biphenylyl)-2-(4-hydroxyphenyl)propane and α,ω-dibromoalkanes with even numbers of methylene units. The detailed synthesis procedure has been reported in an earlier publication.[3] The molecular parameters for even-TPP(n > 8)s are listed in Table 1 [TPP(n = even)s with lower numbers of methylene units cannot be completely dissolved in THF and no GPC data are available]. The sample preparations for various experiments are the same as described in refs 1 and 2.

Instruments and Experiments. The experiments are similar to those reported in refs 1 and 2 and therefore are only briefly described here. Thermal transition behavior was detected *via* a Perkin-Elmer DSC-7 instrument. The DSC temperature and heat flow scales at different cooling rates (2.5−40 °C/min) were carefully calibrated using standard materials. After holding above the melting temperature for 2 min, the samples were cooled below the glass transition temperature for each polymer at different rates followed by consecutive heating at a rate which was equal to or faster than the prior cooling rate. The onset temperature of the transition on the high-temperature side during cooling was determined and used as the transition temperature, while in the heating curves the transition temperature was determined by the onset temperature on the low-temperature side.

A Rigaku 12 kW rotating anode generator (Cu Kα radiation) with a diffractometer was used for WAXD powder experiments. The scanning 2θ angle ranges between 2° and 35°. A hot stage was set up on the diffractometer to measure the phase transition at constant cooling and heating rates of 5 °C/min with a temperature accuracy of better than ±1 °C in the temperature range studied. The thermal histories of the samples were kept the same as those in the DSC experiments. The WAXD fiber patterns of TPP(n = even)s were taken at different temperatures, particularly where the phase transitions occur, on a Siemens two-dimensional area detector. During the measurements, the fiber length was fixed. The Scherrer equation was used, as a first approximation, to calculate the correlation length of the ordered structure perpendicular to the reflection plane *via* the width of the half-peak height of each reflection peak.

Liquid crystalline morphology was observed *via* a PLM instrument (Olympus BH-2) with a Mettler hot stage (FP-82) and a JEOL 1200 EX II TEM instrument. The TEM instrument was operated at an accelerating voltage of 120 kV. For PLM, both isothermal and nonisothermal experiments were performed. The mechanically sheared and unsheared samples were prepared as described previously.[1,2] For TEM observations, the sheared samples were prepared in the same way as in the case of PLM experiments and then physically oversheared to separate the glass slides before they were immediately quenched. The samples were annealed at a temperature of 10−20 °C below the mesophase transition temperature to allow further ordering and/or crystallization and the formation of lamellar crystals to decorate the liquid crystal texture.[11,12] The samples were then shadowed by Pt and coated with carbon for TEM observations. In order to determine the molecular direction, the sheared and coated samples were also directly examined by electron diffraction (ED) experiments under the TEM.

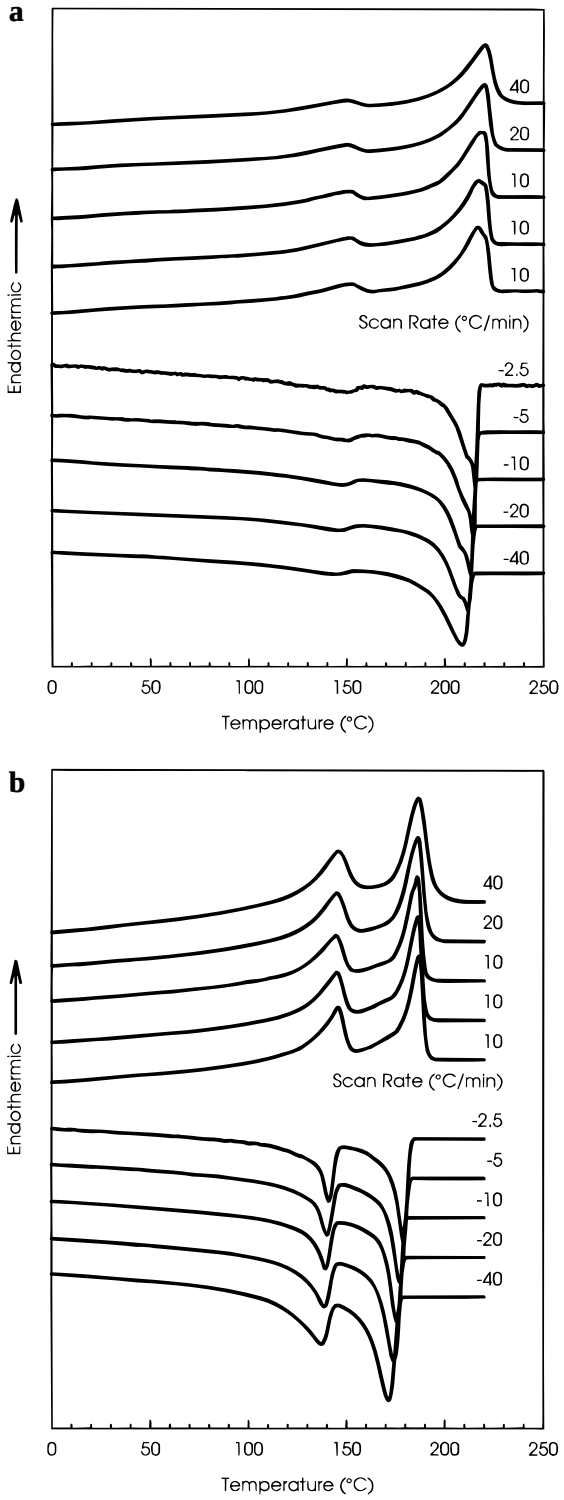

Figure 1. Sets of DSC cooling and heating curves for (a) TPP (n = 8) and (b) TPP(n = 12) at different rates.

Results and Discussion

Equilibrium Phase Transition Temperatures. As two examples, Figure 1 shows two sets of DSC cooling and heating curves for TPP(n = 8 and 12) at different rates exhibiting four and five phase transi-

tions, respectively. These transition temperatures show little undercooling dependence. For instance, the first exothermic transition of TPP(n = 8) occurs at 217 °C having an undercooling dependence of 5 °C in a cooling rate range between 2.5 and 40 °C/min. The second exothermic process is at 211 °C, which overlaps with the first exotherm and also shows an undercooling dependence of 5 °C in the same cooling rate range. The third exothermic process is weak and hidden in the second one. The existence of this process is inherent in the fact that one needs a summation of two asymmetric sigmoidal functions to fit the exothermic process. To quantitatively analyze the change of transition enthalpy, a peak deconvolution program (PeakFit published by Jandel Scientific) has been used based on these functions. The undercooling dependence of this weak transition is again 5 °C in this cooling rate range. The last (lowest) exothermic process occurs at 158 °C, which is evident in the DSC cooling and heating curves (Figure 1a), and shows a 7 °C undercooling dependence with cooling rate. The small undercooling dependence indicates that these transitions are close to the thermodynamic equilibrium.

For TPP(n = 12), similar observations can be made. Five transitions have been identified. The onset transition temperatures are 184, 165, 148, 128, and 101 °C, and the undercooling dependences with the cooling rate range between 2.5 and 40 °C/min are 7, 7, 6, 9, and 8 °C, respectively. This reveals again the close-to-equilibrium nature of these transitions. The second, third, and fifth exothermic peaks during cooling are weak, and their existence is also judged by the deconvolution program based on the asymmetric sigmoidal functions which provide the best unique fit to the whole exothermic process. An additional proof of the existence of these transitions is based on sudden volume changes during the transition.[1] This clearly indicates the feature of a first-order thermodynamic transition.

Furthermore, TPP($n \leq 8$)s show similar thermal transition behavior, and the six polyethers of TPP($n \geq 10$)s form another group which exhibits close transition behavior.[13] In order to provide an overview of the transition behavior in TPP(n = even)s, Figure 2 shows the DSC thermal diagrams for all TPP(n = even)s observed at a cooling rate of 5 °C/min.

Figure 3 is a plot of the transition temperatures of TPP(n = even)s with respect to the number of methylene units. All the transition temperatures are extrapolated to zero cooling (or heating) rate, and therefore, the temperatures in Figure 3 should be very close to the equilibrium transition temperature. This plot can thus serve as the phase diagram of TPP(n = even)s if all the phases are identified (the phase assignments are reserved for later discussion). Of particular interest is that the first- and second-transition temperatures in TPP($n \leq 8$)s are close to one other. For instance, in TPP(n = 4) these two transitions are separated by 12 °C, and the separation decreases to only 6 °C for TPP(n = 8). It seems that these two transitions merge to one process as the number of methylene units reaches 10 (see below). On the other hand, TPP($n \geq 10$)s show new phases in the low-temperature region.

Structure and Order Changes during the Phase Transitions. Figure 4 shows two sets of WAXD powder patterns for TPP(n = 8 and 12) at different temperatures during cooling. These patterns during heating are almost identical with those recorded during cooling, indicating that little undercooling dependence can be found in these transitions. Therefore, we will only discuss the results observed during cooling. In TPP(n = 8) at the highest transition temperature of 217 °C (Figures 1a and 4a), the change of the diffraction patterns from the isotropic melt is noted by a shift of the d-spacing of the halo at *ca.* 2θ = 18° toward a smaller spacing (the 2θ angle shifts to a larger value), as shown in Figure 5. The d-spacing of the 18° halo should be attributed to an average distance between chain molecules in the lateral packing. This shift thus represents a nematic liquid crystalline transition from the isotropic melt (an I → N transition) and has been experimentally observed in several other liquid crystalline polymers.[14−17] The I → N transition can be observed in TPP($n \leq 8$)s, which corresponds to the highest temperature transition in DSC results, and this phase

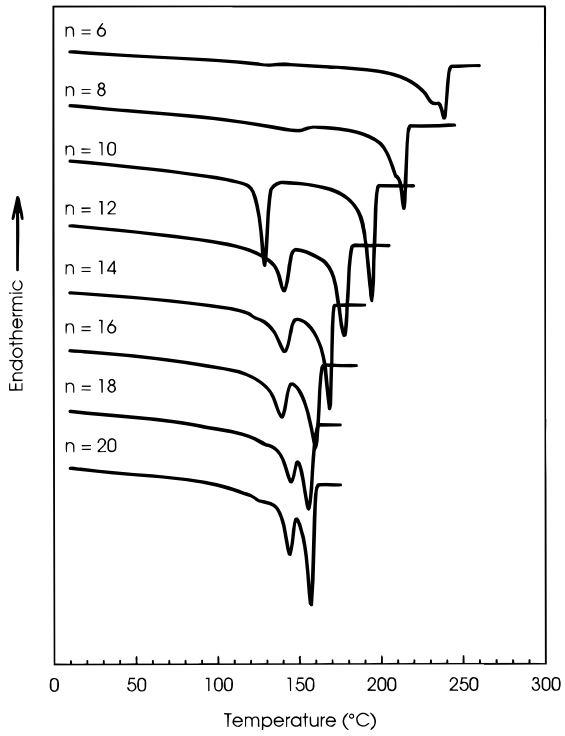

Figure 2. Set of DSC cooling diagrams for TPP(n = even)s at a rate of 5 °C/min.

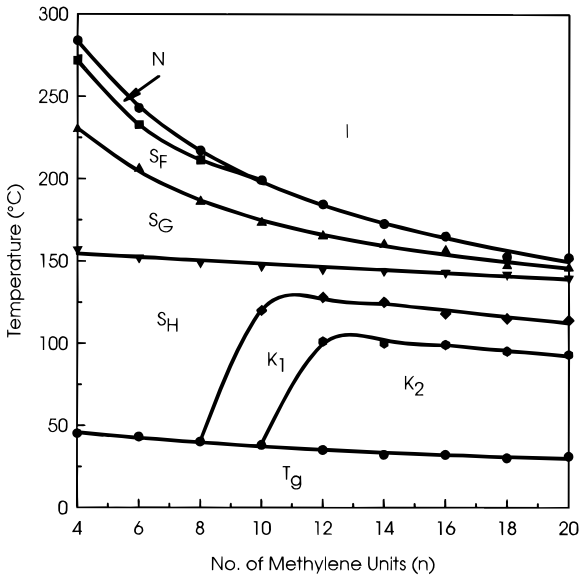

Figure 3. Plot of transition temperature with the number of methylene units for TPP(n = even)s.

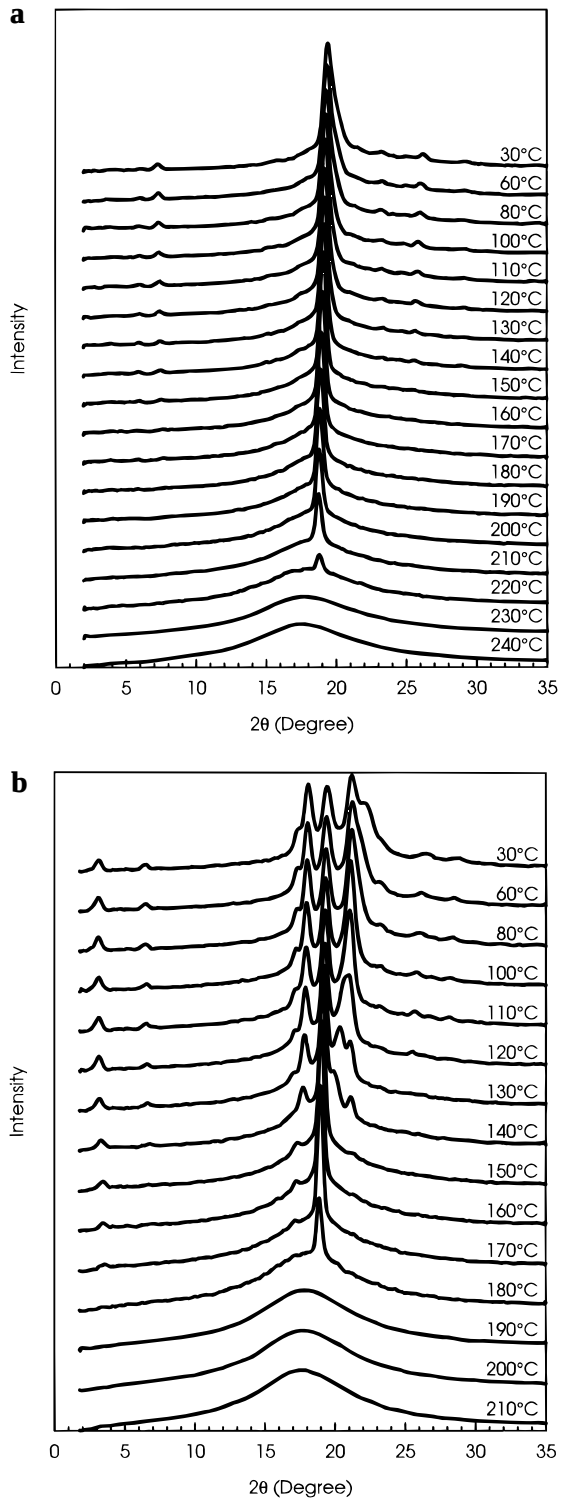

Figure 4. Sets of WAXD powder patterns during cooling from the isotropic melt at 5 °C/min for (a) TPP(n = 8) and (b) TPP(n = 12).

is only stable in a narrow temperature region (Figures 1−4a).

For TPP(n = 8) the immediate appearance of another reflection peak at 2θ = 18.9° occurs when the temperature is decreased to about 210 °C. This represents the second-transition process which is only 6 °C below the first-transition temperature (Figures 1a, 2, and 3). A reflection peak in the low-angle region is diffused in the WAXD powder patterns. Similar observations can also be found in TPP($n \leq 8$)s. The intensity as well as the correlation lengths of this low-angle reflection increases

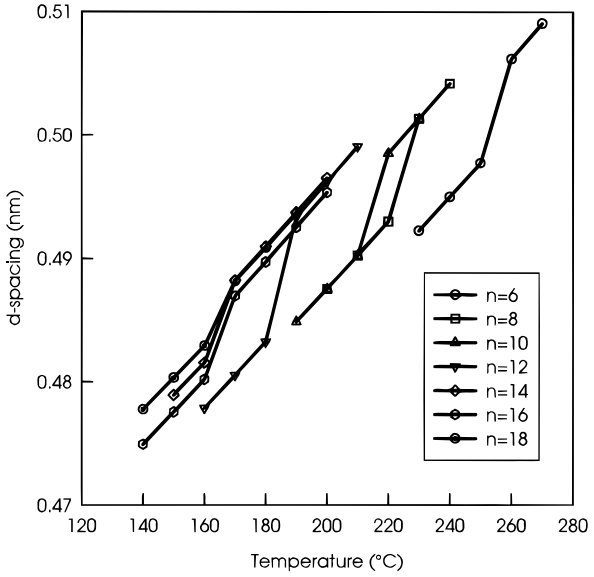

Figure 5. d-Spacing shifts for TPP(n = even)s during the highest transitions observed in DSC (nematic phase formation when $n \leq 8$ and smectic phase formation when $n \geq 10$).

with increasing number of methylene units, indicating that the ordered structure represented by this low-angle reflection peak is enhanced. In contrast, for TPP($n \geq 10$)s the d-spacing shift of the 18° halo is always accompanied by an additional sharp 19° reflection peak. TPP(n = 12) is an example (see Figure 4b). This indicates that a liquid crystalline phase, which possesses an order higher than the S_A or S_C phase, forms directly from the isotropic melt. Furthermore, a low-angle reflection peak can also be observed after the first transition. The relationships of the d-spacing changes in the halo with temperature for TPP($n \geq 10$)s are also plotted with the number of the methylene units and included in Figure 5. Note that a separation of the halo from the 19° reflection peak in these TPPs is carried out in order to construct Figure 5. For TPP($n \geq 10$)s the correlation lengths of the main reflection peaks at around 19° are between 22 and 26 nm[13] and slightly increase with the number of the methylene units. These correlation lengths reveal an existence of long range order. In TPP($n \leq 8$)s, cooling a few degrees from the highest transition temperature also leads to the appearance of a single sharp reflection peak at around 2θ = 19°, which shows the same structural pattern as those observed in TPP($n \geq 10$)s. The correlation length of this reflection peak is around 20 nm, revealing that the ordered structure also possesses a long range order.

Generally speaking, the low-angle reflection peak in WAXD powder patterns should represent a layer spacing in a smectic liquid crystal phase, while the reflection peak that developed at around 2θ = 19° in the high-angle region may be an indication of a smectic phase having a hexagonal (or pseudohexagonal) lateral packing. At this moment, one may conclude that the second transition that appears in DSC for TPP($n \leq 8$)s is a further increase of the structural order to form a phase having hexagonal lateral packing. This phase possesses the same structure as those in TPP($n \geq 10$)s formed after the first (highest) transition temperature.

The third-transition temperature observed from DSC for TPP($n \leq 8$)s and the second-transition temperature for TPP($n \geq 10$)s during cooling both show a relatively small transition enthalpy (between 3 and 8 kJ/mol; see below). Most of the exothermic processes are hidden

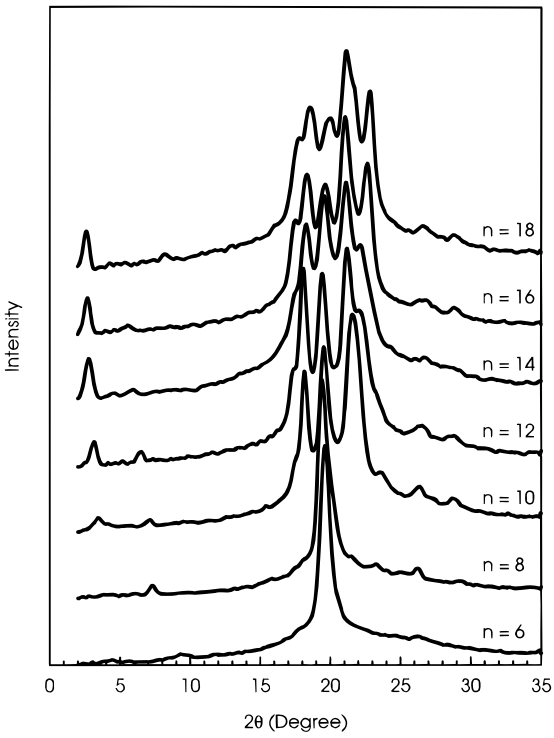

Figure 6. Set of WAXD powder patterns of TPP(n = even)s after they were cooled to room temperature at 5 °C/min.

under the other dominant transition enthalpies. From the WAXD powder patterns, two minor reflections on each side of the main reflection around 19° are found in TPP($n \geq 10$)s. In TPP($n \leq 8$)s these two minor reflections are not as clear as those in TPP($n \geq 10$)s. The low-angle reflection peak remains for all TPP(n = even)s.

The following transition can also be found in all TPP(n = even)s. The WAXD powder patterns exhibit distinct changes. An obvious split of the major reflection peak at around 19° is noted and accompanied by other minor reflections developed in the high-angle region for all TPP($n \geq 10$)s. For TPP($n \leq 8$)s, this split is apparently not clear. However, it may be recognized by a significant decrease (more than 30%) of the correlation length of this reflection during the transition (see below). This indicates a tendency of splitting this major reflection, and therefore, an initiation of the deviation from the hexagonal packing has taken place. The correlation lengths of other reflections, on the other hand, show substantial improvement during the transition, and they are in the long range order. Further cooling leads to a new transition for TPP($n \geq 10$)s, and three reflections are clearly found in addition to the split major reflection peak. For TPP($n \geq 12$)s, another reflection pattern can be observed at even lower temperature, and strong multiple reflections exist. The last two transitions are probably associated with the crystalline phases.

Figure 6 shows the WAXD powder patterns for all TPP(n = even)s after the samples were cooled to room temperature at a cooling rate of 5 °C/min for the purpose of an overview of the ordered structures. It is obvious that two kinds of WAXD patterns can be identified, those in TPP($n \leq 8$)s and those in TPP($n \geq 10$)s. The structure observed for TPP($n \leq 8$)s at room temperature is, in fact, an intermediate order stage appearing in TPP($n \geq 10$)s during cooling. Further ordering processes for TPP($n \leq 8$)s do not proceed since this intermediate ordered structure is stable down to the glass transition temperature, due possibly to the chain rigidity and the resulting limited molecular mobility.

It is, however, difficult to exactly identify the phase structure since WAXD powder patterns do not provide locations of these reflections, and as a result, the dimensionality of the ordered structure cannot usually be determined. The WAXD fiber patterns of TPP(n = even)s are thus necessary to provide detailed phase structural information.

Phase Structure Identifications. Figures 7 and 8 show two sets of WAXD fiber patterns for TPP(n = 8 and 12) at temperatures which are several degrees below each transition temperature observed in DSC, respectively. Although these sets of experiments were carried out during heating, we are going to start our discussion from the high-temperature side in order to match the sequence of other experimental descriptions. For TPP(n = 8), when the temperature is reduced to 205 °C (Figure 7a), a low-angle reflection at $2\theta = 6.0°$ appears, corresponding to a d-spacing of 1.47 nm. The angle between this reflection and the meridianal direction is 52°, revealing that the normal direction of the layer structure in this smectic phase is tilted 52° from the fiber direction (and, also, the chain direction in this case). The correlation length is in a quasi-long range order but cannot be quantitatively measured due to the weak reflection intensity. Another reflection is also found in the high-angle region and is on the equatorial at $2\theta = 18.8°$ (d-spacing of 0.47 nm). This single reflection peak is a clear indication of a hexagonal packing and should be attributed to both the 110 and 100 reflections (the 200 reflection if a monoclinic lattice is used; see below). Furthermore, the correlation length of this reflection is 18 nm, indicating a long range order existing in the lateral packing direction. [Note that this reflection will be split if the lattice deviates from hexagonal packing to become two separated 110 and 200 reflections in an orthorhombic ($\beta = 90°$) or a monoclinic ($\beta \neq 90°$) packing.] As a result, this phase should possess a smectic phase having a structural order higher than the S_C phase. Since the layer normal is tilted from the chain direction, this hexagonal packing is thus converted into a monoclinic lattice. Based on the experimental reflection data, dimensions of a S_F monoclinic unit cell in TPP(n = 8) can be calculated to be a = 1.53 nm, b = 0.55 nm, c = 2.39 nm, and $\beta = 142°$. The schematics of chain packing and morphology in S_F are shown in Figure 7d as an example. However, in TPP(n = even)s the molecular and fiber axes are parallel to each other; it is important to look for other reflections in the quadrant to support this phase structure assignment. This phase may also be assigned as a smectic I (S_I) phase, which is distinguished by the tilting direction of the chain molecules toward a side (S_F) or an apex (S_I). Nevertheless, the relative deviation between calculated and observed d-spacings after refinement (which is $\Sigma|\Delta d|/(\Sigma d)$, where Δd is the difference between calculated and observed d-spacings) for the S_I phase in TPP(n = even)s is more than 2 orders of magnitude greater than that of the S_F phase (see below), indicating that for TPP(n = even)s this liquid crystalline state should be a S_F phase.

At a temperature of 180 °C for TPP(n = 8), which is in between the third and fourth transitions as shown in Figure 2, the WAXD fiber pattern (Figure 7b) shows a very similar observation as in the case of Figure 7a. The only difference is that the overlapped 110 and 200

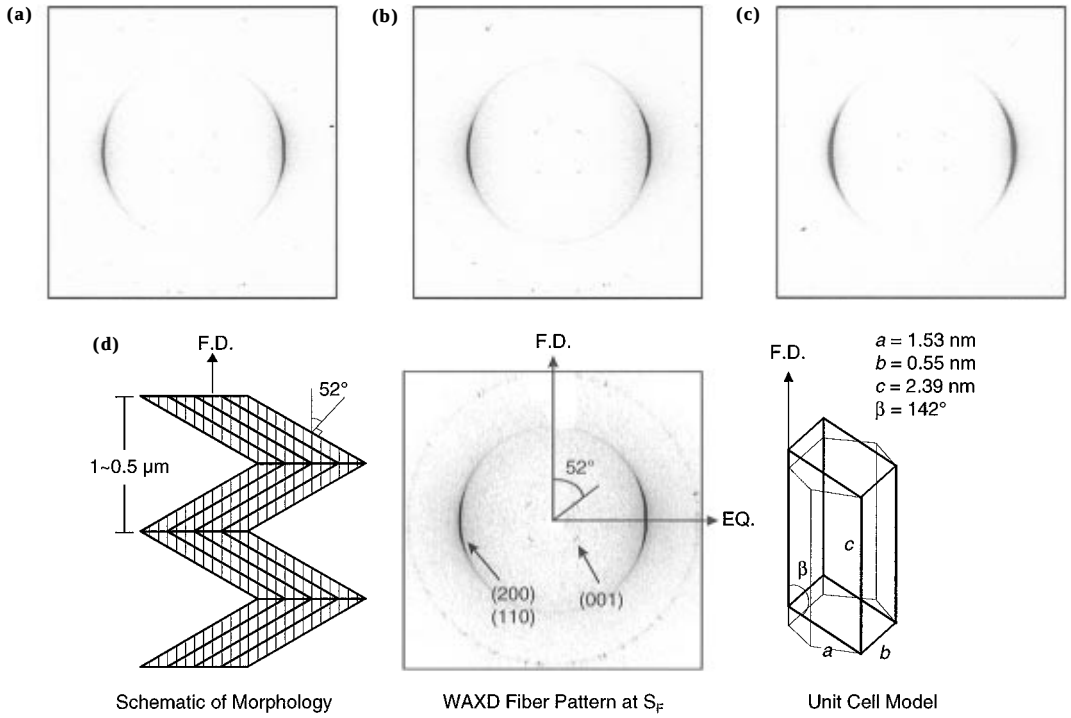

Figure 7. Sets of WAXD fiber patterns for TPP(n = 8) at (a) 205, (b) 180, and (c) 150 °C, which are 5 °C below the transition temperatures observed in DSC. (d) Schematics of morphology, (*hkl*) assignment for fiber pattern, and a unit cell model for the S_F phase. (FD is fiber direction and EQ equatorial direction.)

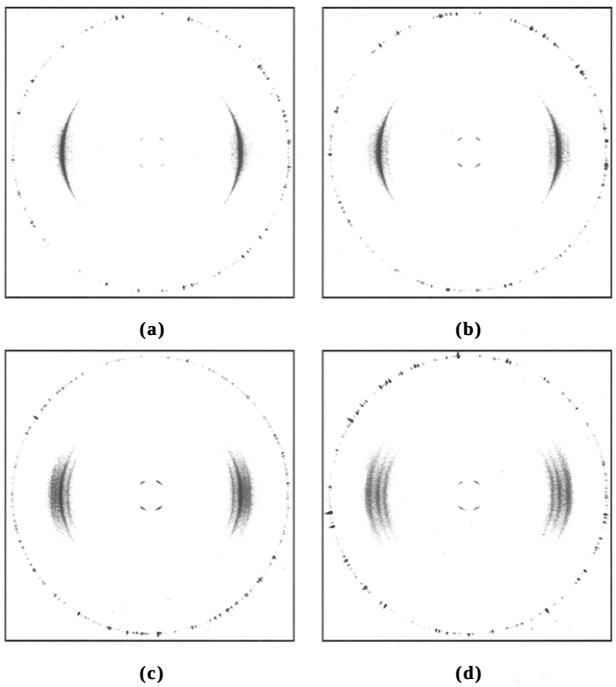

Figure 8. Sets of WAXD fiber patterns for TPP(n = 12) at (a) 180, (b) 160, (c) 145, and (d) 125 °C, which are 5 °C below the transition temperatures observed in DSC.

reflections in the monoclinic unit cell are slightly shifted to a larger angle (2θ = 19.0° versus 18.8° previously). This leads to a slight change of the unit cell dimensions of a = 1.52 nm and b = 0.54 nm. However, their correlation lengths are improved to 20 nm as compared with those in the S_F phase of 18 nm, indicating an increase of the lateral structure order within the layers. Furthermore, the layer correlation order is 10 nm, which is just into the long range order region compared with that of the quasi-long range order in the S_F phase. These characteristics are perhaps the most important structural evidence to prove the phase transition of $S_F \rightarrow S_G$ besides the sudden change of unit cell volume at the transition. This also corresponds to the weak enthalpy change during the transition as observed in DSC experiments.

When the temperature is below the transition temperature of 158 °C, the WAXD fiber pattern of TPP(n = 8) in Figure 7c shows not only the same low-angle reflection at 2θ = 6.0° with a 52° tilt angle from the meridian and a correlation length of 12 nm but also four reflections in the high-angle region. The 110 and 200 reflections in this monoclinic lattice are now separated from each other at 2θ = 19.4° and 20.3° (d-spacings of 0.46 and 0.44 nm, respectively), indicating a deviation from the hexagonal packing viewing along the chain direction toward an orthorhombic lattice. The correlation lengths are 20 and 18 nm, respectively. The third reflection is seen on the equatorial at 2θ = 26.1° (d-spacing of 0.34 nm) and is determined to be the 210 reflection with a correlation length of 12 nm. The fourth reflection is on the first layer in the quadrant at 2θ = 23.1° (d-spacing of 0.38 nm) and assigned to be the $(\bar{2}11)$ planes with a correlation length of 11 nm. Again, the chain direction is tilted toward a side. Monoclinic lattice dimensions can determined as a = 1.42 nm, b = 0.54 nm, c = 2.39 nm, and β = 142°. This phase can thus be identified as a smectic crystal H (S_H) phase. To summarize all the transitions observed in TPP(n = 8), they show that

$$I \xrightarrow{217°C} N \xrightarrow{211°C} S_F \xrightarrow{186°C} S_G \xrightarrow{158°C} S_H$$

This phase identification for TPP(n = 8) can be generalized to TPP($n \leq 8$)s.

In contrast, for TPP(n = 12) the WAXD fiber patterns (Figure 8) show that below the highest transition temperature (184 °C), one low-angle reflection at 2θ = 3.6° (d-spacing of 2.42 nm) can be found (Figure 8a) and assigned as the 001 reflection. It is tilted from the

meridian direction by an angle of 35°, indicating that the layer structure is tilted 35° from the chain direction which is parallel to the fiber direction. Its correlation length is 10 nm, which is at the borderline between quasi-long range and long range orders along the layer structure. One set of high-angle reflections appears on the equatorial at $2\theta = 19.0°$. Again, this is attributed to two overlapped 110 and 100 reflections of a hexagonal packing when one views parallel to the chain axis (the 100 reflection will be converted to the 200 reflection in a monoclinic unit cell). The correlation length is 22 nm. Two reflections are on the first layer in the quadrant at $2\theta = 17.2°$ and 21.4° (d-spacings of 0.52 and 0.42 nm, respectively). Their correlation lengths are 13 and 11 nm. They are assigned as the $\bar{2}01$ and 201 reflections. A monoclinic lattice with dimensions of $a = 1.14$ nm, $b = 0.54$ nm, $c = 3.00$ nm, and $\beta = 125°$ is determined. Similar to the structural identification in TPP($n = 8$), this phase can be classified as the S_F phase. Another possibility is that this phase is assigned as a S_I phase, and therefore, the dimensions should be $a = 0.68$ nm, $b = 0.93$ nm, $c = 2.95$ nm, and $\beta = 125°$. The $\bar{2}01$ and 201 reflections in the S_F phase now become the $\bar{1}11$ and 111 reflections. The relative deviation of the S_I phase is 5.5%, while that of the S_F phase is 0.03%, indicating a 2 orders of magnitude difference. As a result, the assignment of a S_F phase for TPP($n = 12$) is justified.

When reducing the temperature below 165 °C (Figure 8b), all the reflections remain as shown in Figure 8a. The high-angle reflection positions shift slightly toward larger 2θ angles, and the low-angle reflection is slightly moved to a smaller angle (increasing the d-spacing). The major difference is in the correlation lengths of these reflections. All of them are increased by at least 14%, indicating a significant improvement of the lattice order in the structure. For example, the correlation length of the 110 and 200 reflections is 26 nm in this phase compared with that of 22 nm in S_F phase. Based on the calculation, a S_G phase with $a = 1.14$ nm, $b = 0.54$ nm, $c = 3.17$ nm, and $\beta = 125°$ can be obtained.

When the third transition at 148 °C is passed, the WAXD fiber pattern (Figure 8c) shows the low-range layer reflections (the 001 and 002 reflections) which are tilted away from the meridian direction of 35°. We still experimentally observe one reflection on the equatorial at $2\theta = 19.2°$ (d-spacing of 0.46 nm), indicating that the lateral packing of the chain molecules is close to hexagonal. This reflection apparently represents the overlapped 110 and 100 reflections in the hexagonal packing. Three reflections are on the first layer in the quadrant: the ($\bar{2}01$), (111), and (201) planes at $2\theta = 17.8°$, 20.4°, and 21.1° (d-spacings of 0.50, 0.44, and 0.42 nm, respectively). One reflection, the $\bar{2}02$, is on the second layer of the quadrant at $2\theta = 17.0°$ (d-spacing of 0.52 nm). Besides the 110 and 100 reflections, the correlation lengths for all other reflections show a 12−15% increase, revealing a long range ordered structure within the layers. However, the correlation length of the overlapped 110 and 100 reflections shows a significant drop from 26 nm in the S_G phase to 18 nm in this phase, which represents a decrease of more than 30%. This indicates that although the separation of the 110 and 200 reflections is not observed within the experimental resolution, the decrease in the correlation length clearly shows that the lateral lattice packing starts deviating from the hexagonal packing and toward an orthorhombic lattice when the viewing direction is parallel to the chain axis. Detailed calculation to fit all these reflections into a lattice yield a monoclinic unit cell of $a = 1.08$ nm, $b = 0.53$ nm, $c = 3.27$ nm, and $\beta = 121°$. Since the lattice viewed parallel to the chain direction is approaching an orthorhombic lattice, this phase can be assigned as a S_H crystal phase.

Further decreasing the temperature leads to two crystalline phases, K_1 and K_2 (Figure 8d). Both of these phases exhibit monoclinic packing with similar lattice structures. One of the differences that can be found during the $K_1 \rightarrow K_2$ transition is an improvement of correlation lengths for all the reflections by at least 5%, and all of the correlation lengths correspond with long range order. Since we are focusing on the highly ordered smectic liquid crystalline phases in these TPP(n = even)s, detailed crystallographic analyses for these structures are offered elsewhere.[13] The phase transition in TPP($n = 12$) can thus be summarized as

$$\mathrm{I} \xrightarrow{184°\mathrm{C}} \mathrm{S_F} \xrightarrow{165°\mathrm{C}} \mathrm{S_G} \xrightarrow{148°\mathrm{C}} \mathrm{S_H} \xrightarrow{128°\mathrm{C}} \mathrm{K_1} \xrightarrow{101°\mathrm{C}} \mathrm{K_2}$$

For TPP($n \geq 10$)s, similar phase transition behavior is seen as in the case of TPP($n = 12$).

Morphological Evidence of the Phase Transitions. Figure 9 shows PLM morphological observations of TPP($n = 8$ and 12) without and with mechanical shearing. During the nonisothermal experiments cooled from the isotropic melt, the samples immediately become birefringent after a few seconds at the highest transition temperature. A fine, grainy texture is observed (Figure 9a,c). After the mechanical shearing and slight relaxation at the transition temperature, banded textures can be found in TPP($n = 8$) (Figure 9b), although the banded texture seen is not as clear as those observed in the odd-numbered TPP($n \leq 13$)s.[2] This banded texture possesses a spacer of 0.5−1 μm perpendicular to the shearing direction and has been viewed as a typical morphological texture of the low-ordered liquid crystal polymers in N, S_A, and S_C phases.[1,2,16−18] Microscopic analysis has shown that in the banded texture, the director continuously oscillates spatially about the direction imposed by the previous flow. This texture can also be formed in other even-TPP($n \leq 8$)s when the samples were sheared at the highest transition temperature. However, this type of banded texture cannot be found in sheared TPP($n \geq 10$)s since this polymer possesses a direct transition from the isotropic melt to the S_F phase. Instead, we have observed that as soon as the $I \rightarrow S_F$ transition takes place, the liquid crystalline morphology under PLM is very similar to those observed in odd-TPP($n \geq 15$)s (Figure 9d).[2] This indicates that a highly ordered smectic phase forms. Furthermore, the sample immediately losses its fluidity and turns into a solid-like material. Sometimes, a broken texture can be seen. Further decreases in the temperature do not lead to a significant PLM texture change. Only minor birefringence changes are observed. This indicates that the ordered structure change occurs at even smaller dimensional scale (within micrometer size), and TEM study is necessary to observe the morphological changes accompanied with the phase transitions.

Using the "lamellar decoration method"[11,12] originally developed by Thomas *et al.*, typical liquid crystal defect patterns seen under TEM are observed as shown in Figure 10 for mechanically sheared TPP($n = 8$ and 12) thin film samples. It should be pointed out that one needs to know the relationship between the observed morphology at room temperature and that of the phases

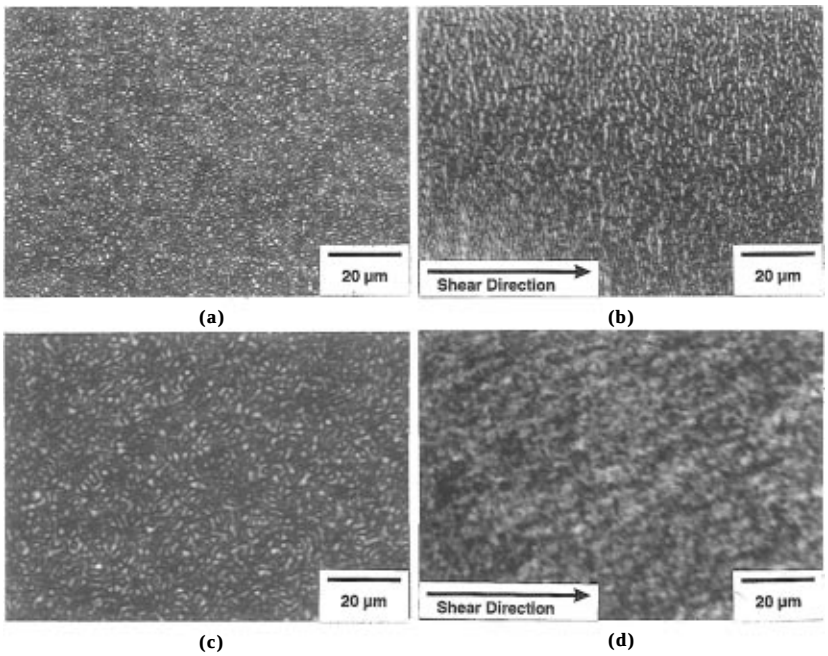

Figure 9. Set of PLM morphological observations of (a) TPP($n = 8$) without shearing, (b) TPP($n = 8$) with mechanical shearing, (c) TPP($n = 12$) without shearing, and (d) TPP($n = 12$) with mechanical shearing.

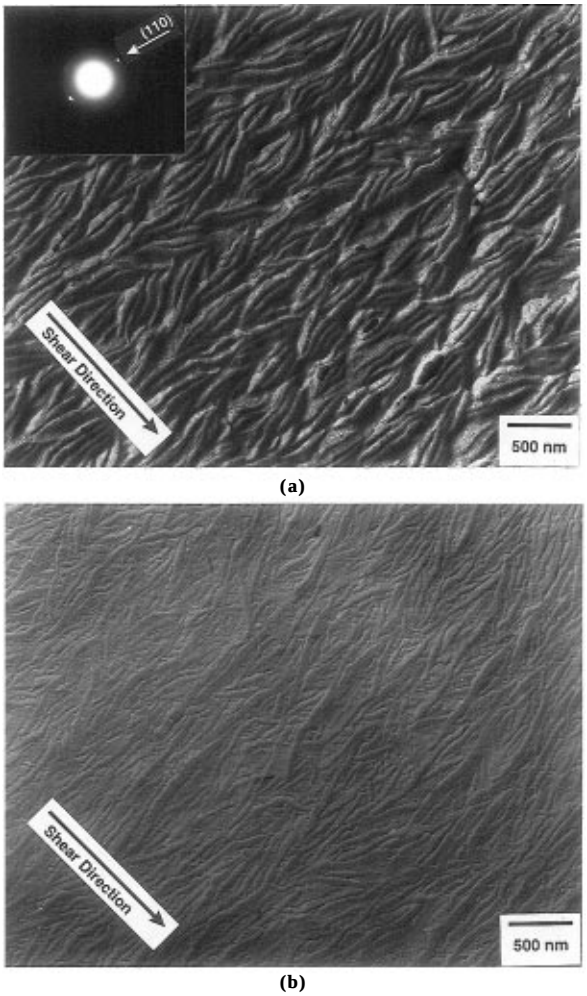

Figure 10. TEM observation of (a) TPP($n = 8$) and (b) TPP($n = 12$) after lamellar decoration.

formed at high temperatures since these phase transitions are close to thermodynamic equilibrium and are difficult to be bypassed even during quenching. This has been simplified because from the PLM observations no liquid crystalline texture change can be found down to the micrometer size scale. Therefore, the TEM observations at room temperature should resemble the topological texture in the S_F phase except for the slight change of unit cell dimensions and the change of correlation length.

If one compares the morphologies between TPP($n = 8$) where the nematic phase formed first from the isotropic melt and TPP($n = 12$) where the S_F phase is directly formed from the isotropic melt under shear (Figure 10, the shear direction is indicated), it is evident that these two morphological observations do provide significant differences due to the presence of the banded texture in TPP($n = 8$) but not in TPP($n = 12$). For TPP($n = 8$), the lamellar normal direction is roughly about 50−60° with respect to the shear direction, and it is responsible for the four-point quadrant reflections in the low-angle region observed from the WAXD fiber pattern (Figure 7b−d). The spacing of about 0.5−1 μm for TPP($n = 8$) in the TEM observations clearly corresponds to the banded texture found in PLM (Figure 9b). The shear direction is interestingly perpendicular to the layer texture as indicated by the ED pattern in Figure 10a. Furthermore, the *d*-spacing and location of the reflection spots in the ED pattern are essentially the same for the 110 reflection as those found in the WAXD fiber pattern in Figure 8d. This indicates that the local orientation and order are the same as the overall ones detected *via* WAXD experiments. Finally, for both TPP cases, the average lamellar spacing is *ca.* 25 nm, and this size fits well with the correlation lengths obtained from the WAXD experiments, which are in the vicinity of 15−30 nm for TPP($n = 8$ and 12) in the S_H and crystal phases at room temperature.

Phase Diagram of TPP(n = even)s. On the basis of DSC, WAXD, PLM, and TEM experimental observations, we can clearly assign the phases in TPP(n = even)s following the sequence from high to low temperatures. For TPP($n \leq 8$)s, the first (and the highest) transition is the I → N transition, and the temperature range for the nematic phase is narrow. With decreasing temperature, the N → S_F phase transition can be

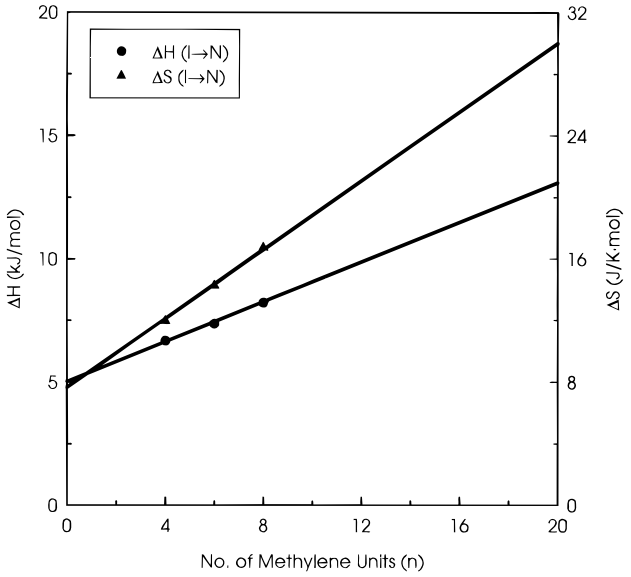

Figure 11. Relationships between the ΔH_{IN} and ΔS_{IN} during the I → N transition observed in DSC and the number of methylene units for TPP($n \leq 8$)s.

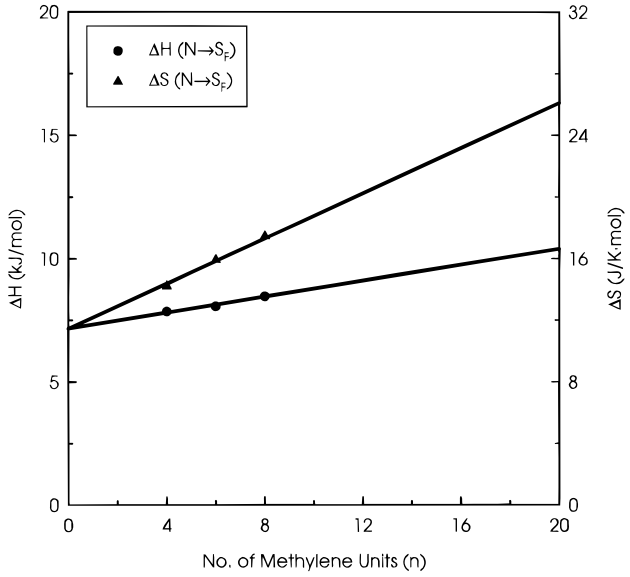

Figure 12. Relationships between the ΔH_{NF} and ΔS_{NF} during the N → S_F transition observed in DSC and the number of methylene units for TPP($n \leq 8$)s.

identified. In contrast, for TPP($n \geq 10$)s the transition from the I → S_F phase is observed during the highest temperature transition, and no I → N transition can be seen. Further decreasing the temperature leads to a transition behavior of the S_F → S_G phases for all TPP(n = even)s followed by another transition of S_G → S_H phases. Two phase transitions can also be identified during further cooling for TPP($n \geq 10$)s, which are the S_H → K_1 and K_1 → K_2 crystal phase transitions. Figure 3 includes the phase assignments and serves as a complete phase diagram for TPP(n = even)s.

Now we turn to the discussion of the thermodynamic parameters of the transitions in TPP(n = even)s. In principle, the enthalpy and entropy changes of transitions (ΔH and ΔS) can be plotted with respect to the number of methylene units [the transition entropy change (ΔS) is calculated based on the known equilibrium transition temperatures *via* $\Delta S = \Delta H/T$]. Approximately linear relationships can be found in a range of the even-numbered TPP($4 \leq n \leq 20$)s, similar to the TPP(n = odd)s as well as several other liquid crystalline polymers.[2,15,17,19−21] The slopes of these linear relationships may represent the ΔH and ΔS contributions to the transition per mole of methylene units, while the interceptions are roughly attributed to the transition ΔH and ΔS per mole of mesogenic groups. Figures 11 and 12 are these plots for the I → N and the N → S_F transitions for TPP($n \leq 8$)s. For TPP($n \geq 10$)s, the highest transition is from the isotropic melt directly to the S_F phase. It is assumed that the summations of both transition enthalpies and entropies of the I → N and N → S_F in TPP($n \leq 8$)s should fit into the linear relationships of the transition ΔH and ΔS with the methylene units for the I → S_F transitions in TPP($n \geq 10$)s (additive scheme). This is indeed the case as shown in Figure 13, which, in turn, provides indirect evidence that the assignment of the S_F phase in TPP($n \leq 8$)s is correct. Figures 14 and 15 show the same relationships for the S_F → S_G and S_G → S_H transitions. The interceptions of the ΔH_{GH} and ΔS_{GH} are not close to zero after the extrapolation to zero number of methylene units, indicating that this phase transition involves both ordering processes attributed to the methylene units and the mesogenic groups. Detailed values of the slopes

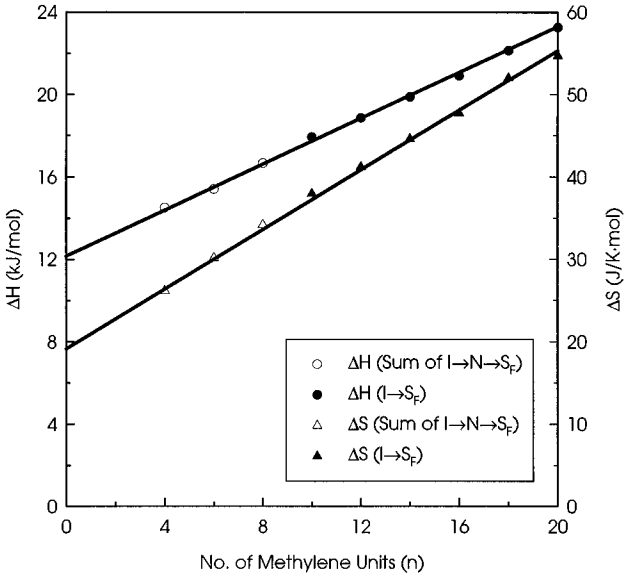

Figure 13. Relationships between the ΔH_{IF} and ΔS_{IF} during the I → S_F transition observed in DSC and the number of methylene units for TPP(n = even)s. (Note that these data for TPP($n \leq 8$)s are the summation of both contributions from the I → N and N → S_F transitions; see text.)

and intersections for all the liquid crystalline transitions shown in Figures 11−15 are listed in Table 2. In this table, a parallel list of the TPP(n = odd)s is also included for comparison.[2,13]

Many discussions can be carried out based on the data listed in Table 2. We only focus on a few of the interesting features in this publication. First, the I → N transition in TPP(n = odd)s shows much less orientational order compared with that in TPP(n = even)s. In particular, the transition enthalpy change contributed from the mesogenic groups in TPP(n = even)s is 3 times greater than that in TPP(n = odd)s, while the transition enthalpy change from the methylene units in TPP(n = even)s is only 63% of that in TPP(n = odd)s. The same trend can be found in the transition entropy changes. Second, for the formation of the S_F phase, the mesogenic group contribution in TPP(n = even)s is almost 6 times greater than that in TPP(n = odd)s,

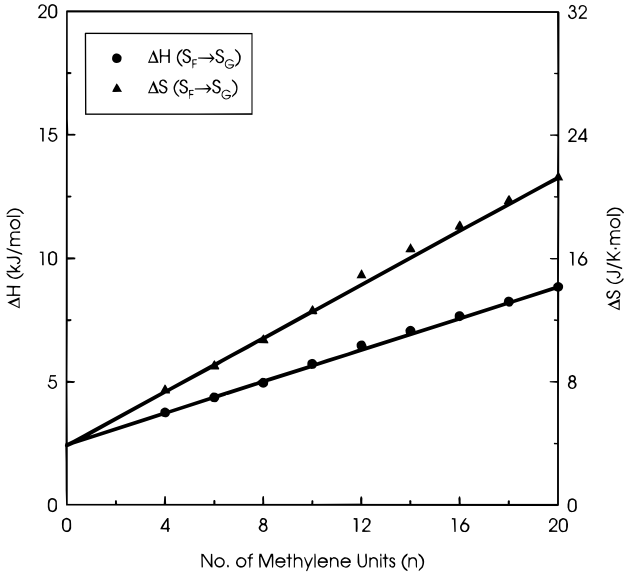

Figure 14. Relationships between the ΔH_{FG} and ΔS_{FG} during the $S_F \rightarrow S_G$ transition observed in DSC and the number of methylene units for TPP(n = even)s.

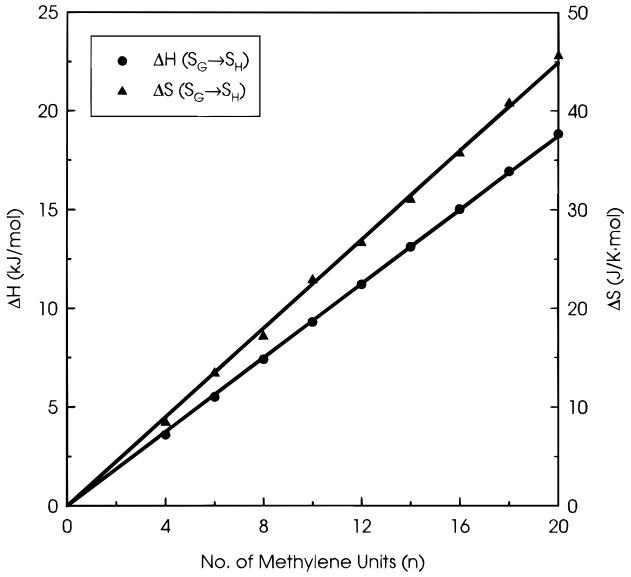

Figure 15. Relationships between the ΔH_{GH} and ΔS_{GH} during the $S_G \rightarrow S_H$ transition observed in DSC and the number of methylene units for TPP(n = even)s.

Table 2. Transition Enthalpy and Entropy Changes for Methylene Units and Mesogenic Groups for the Liquid Crystalline Transitions

	ΔH (kJ/mol)		ΔS (J/K·mol)	
transition	mesogene	methylene	mesogene	methylene
		Odd		
$I \rightarrow N$	1.64	0.63	2.80	1.54
$N \rightarrow S_F$	0.50	0.43	1.78	0.96
$I \rightarrow S_F$	2.14	1.06	4.58	2.50
$S_F \rightarrow S_G$	≈0.00	0.42	≈0.00	1.04
$S_G \rightarrow S_H$	≈0.00	0.92	≈0.00	2.35
		Even		
$I \rightarrow N$	5.01	0.40	7.65	1.12
$N \rightarrow S_F$	7.15	0.16	11.43	0.73
$I \rightarrow S_F$	12.16	0.56	19.14	1.81
$S_F \rightarrow S_G$	2.45	0.32	3.85	0.89
$S_G \rightarrow S_H$	≈0.00	0.95	≈0.00	2.25

while for TPP(n = even)s the methylene unit contribution is only one-half that of TPP(n = odd)s. Third, the formation of the S_G phase shows that the mesogenic groups still possess a contribution in TPP(n = even)s, while this is not the case in TPP(n = odd)s [in which both $\Delta H(S_F \rightarrow S_G)$ and $\Delta S(S_F \rightarrow S_G)$ for the mesogenic groups are very close to zero (Table 2)]. On the other hand, the methylene unit contributions for this transition in TPP(n = even)s are roughly 70−80% of those in TPP(n = odd)s. Finally, the contributions of the mesogenic groups and methylene units to the enthalpy and entropy changes in the $S_G \rightarrow S_H$ transitions for both TPP(n = odd) and TPP(n = even) series do not show significant differences. Overall, it is evident that the mesogenic groups and methylene units in this series of TPP(n = even)s may play different roles to stabilize the liquid crystalline phases compared with those of TPP(n = odd)s. Detailed molecular motion and chain conformation analysis are required to conduct further discussion.

Conclusion

A phase diagram of TPP(n = even) polyethers has been established. The complicated phase assignments are based on different experimental observations. The phase transitions are observed *via* DSC experiments, which provide fundamental understandings of the phase stability and transition thermodynamics and serve as additional proof of the phase assignments. The essential structural information has, however, to be obtained through WAXD powder and fiber patterns at different temperatures. Liquid crystalline structure and morphology observed *via* PLM and TEM as well as ED experiments are also useful to identify these different phases. It is particularly interesting that this series of main-chain liquid crystalline TPPs exhibits the highly ordered smectic phase (S_F) and smectic crystal phase (S_G or S_H). These results indicate that a careful examination of the liquid crystalline structures is the key to identifying these mesophases, which are closely associated with the phase definitions in small molecule liquid crystals.

Acknowledgment. This research was supported by a Presidential Young Investigator Award (DMR-9157738) to S.D.Z.C.

References and Notes

(1) Cheng, S. Z. D.; Yoon, Y.; Zhang, A.; Savitski, E. P.; Park, J.-Y.; Percec, V.; Chu, P. *Macromol. Rapid Commun.* **1995**, *16*, 533.
(2) Yoon, Y.; Zhang, A.; Ho, R.-M.; Cheng, S. Z. D.; Percec, V.; Chu, P. *Macromolecules* **1995**, *29*, 294.
(3) Percec, V.; Chu, P. Ungar, G.; Cheng, S. Z. D.; Yoon, Y. *J. Mater. Chem.* **1994**, *4*, 719.
(4) Yoon, D. Y.; Masciocchi, N.; Depero, L. E.; Viney, C.; Parrish, W. *Macromolecules* **1990**, *23*, 1793.
(5) Coassolo, A.; Foá, M.; Dainelli, D.; Scordamaglia, R.; Barino, L.; Chapoy, L. L.; Rustichelli, F.; Yang, B.; Torquati, G. *Macromolecules* **1991**, *24*, 1701.
(6) Carotenuto, M.; Iannelli, P. *Macromolecules* **1992**, *25*, 4373.
(7) de Gennes, P. G.; Prost, J. *The Physics of Liquid Crystals*; Clarendon: New York, 1993.
(8) The precise definition of long range order in small molecules should be that the translational correlation persists over essentially the entire sample having Bragg peaks which are δ function spikes. The quasi-long range order, on the other hand, should be represented by the Bragg peaks being power-law singularities.
(9) Gray, G. W.; Goodby, J. W. G. *Smectic Liquid Crystals*; Leonard Hill: London, 1984.
(10) Pershan, P. S. *Structure of Liquid Crystal Phases*; World Scientific: River Edge, NJ, 1988.

(11) Thomas, E. L.; Wood, B. A. *Faraday Discuss. Soc.* **1985**, *79*, 229.
(12) Wood, B. A.; Thomas, E. L. *Nature* **1986**, *324*, 655.
(13) Yoon, Y. Ph.D. Dissertation, Department of Polymer Science, The University of Akron, Akron, OH, 44325-3909, 1995.
(14) Ungar, G.; Feijoo, J. L.; Keller, A.; Yourd, R.; Percec, V. *Macromolecules* **1990**, *23*, 244.
(15) Yandrasits, M. A.; Cheng, S. Z. D.; Zhang, A.-Q.; Cheng, J.-L.; Wunderlich, B.; Percec, V. *Macromolecules* **1992**, *25*, 2112.
(16) Pardey, R.; Harris, F. W.; Cheng, S. Z. D.; Aducci, J.; Facinelli, J. V.; Lenz, R. W. *Macromolecules* **1992**, *25*, 5060.
(17) Pardey, R.; Harris, F. W.; Cheng, S. Z. D.; Aducci, J.; Facinelli, J. V.; Lenz, R. W. *Macromolecules* **1993**, *26*, 3687.
(18) Chen, J.-H.; Zhang, A.-Q.; Yandrasits, M. A.; Cheng, S. Z. D.; Percec, V. *Makromol. Chem.* **1993**, *194*, 3135.
(19) Blumstein, A.; Thomas, O. *Macromolecules* **1982**, *15*, 1264.
(20) Blumstein, R. B.; Stickles, E. M.; Blumstein, A. *Mol. Cryst. Liq. Cryst. (Lett.)* **1982**, *82*, 205.
(21) Blumstein, R. B.; Blumstein, A. *Mol. Cryst. Liq. Cryst.* **1988**, *165*, 361.

MA951746Y